# Structural and Dynamic Characterization of the Interaction of the Putative Fusion Peptide of the S2 SARS-CoV Virus Protein with Lipid Membranes

**Jaime Guillén,[†] Rodrigo F. M. de Almeida,[‡,§] Manuel Prieto,[‡] and José Villalaín*[,†]**

*Instituto de Biología Molecular y Celular, Universidad Miguel Hernández, E-03202, Elche-Alicante, Spain, Centro de Química-Física Molecular, Instituto Superior Técnico, 1049-001 Lisboa, Portugal, and Centro de Química e Bioquímica, Faculdade de Ciências da Universidade de Lisboa, 1749-016 Lisboa, Portugal*

*Received: December 17, 2007; Revised Manuscript Received: March 1, 2008*

The SARS coronavirus (SARS-CoV) envelope spike (S) glycoprotein, a Class I viral fusion protein, is responsible for the fusion between the membranes of the virus and the target cell. In the present work, we report a study of the binding and interaction with model membranes of a peptide pertaining to the putative fusion domain of SARS-CoV, $SARS_{FP}$, as well as the structural changes that take place in both the phospholipid and the peptide molecules upon this interaction. From fluorescence and infrared spectroscopies, the peptide ability to induce membrane leakage, aggregation and fusion, as well as its affinity toward specific phospholipids, was assessed. We demonstrate that $SARS_{FP}$ strongly partitions into phospholipid membranes, more specifically with those containing negatively charged phospholipids, increasing the water penetration depth and displaying membrane-activity modulated by the lipid composition of the membrane. Interestingly, peptide organization is different depending if $SARS_{FP}$ is in water or bound to the membrane. These data suggest that $SARS_{FP}$ could be involved in the merging of the viral and target cell membranes by perturbing the membrane outer leaflet phospholipids and specifically interacting with negatively charged phospholipids located in the inner leaflet.

## Introduction

Severe acute respiratory syndrome (SARS) is an atypical pneumonia caused by a newly discovered virus denominated SARS coronavirus (SARS-CoV). Phylogenetic analysis of the amino acid sequence and complete sequencing of this coronavirus [1,2] has shown it to be distinct from previously characterized groups of coronaviruses; SARS-CoV is distantly related to coronavirus group 2 and is therefore classified as a new subfamily within this group. Whereas most coronavirus infections are mild, the mortality rate for SARS-CoV is commonly referred to be about 10% but increases to greater than 50% in persons older than age 60. At present, there is no vaccine available against any human coronavirus infection. Although SARS has been successfully restrained, re-emergence from animal reservoirs is still a potential risk for future recurrences, which is supported by continual reports that find SARS-CoV in small animals, such as civets, raccoon dogs, and bats.[3] Furthermore, evidence of SARS-CoV infection has also been observed in many other marketplace species in China, including cat, red fox, and the Chinese ferret badger.

Coronaviruses are a diverse group of enveloped, positive-stranded RNA viruses with 3–4 proteins embedded in the envelope that cause respiratory and enteric diseases in humans and other animals. SARS-CoV infection, which is similar to other envelope viruses, is achieved through fusion of the lipid bilayer of the viral envelope with the host cell membrane. The spike glycoprotein S, which is responsible for the characteristic spikes of the SARS-CoV, is a surface glycoprotein that mediates viral entry by binding to the cellular receptors ACE2 and CD209L[4,5] and induces membrane fusion. In some strains, protein S is cleaved by a protease to yield two noncovalently associated subunits, S1 and S2 (Figure 1), but cleavage is not an absolute requirement for the mechanism of fusion.[6] The receptor binding domain, localized in domain S1, defines the host range of the virus, and S2 is responsible for the fusion between the viral and cellular membranes.[2,7] S2 contains two highly conserved heptad repeat regions (HR1 and HR2; see Figure 1A),[8–10] which is similar to other viral fusion proteins, including HIV-1 gp41, influenza hemagglutinin HA2, Ebola virus glycoprotein, and paramyxovirus F protein.[11,12] All of them have been classified as class I transmembrane glycoproteins and are displayed on the surface of the viral membrane as oligomers. Class I viral proteins also contain a hydrophobic region denominated as the fusion peptide (FP) and another hydrophobic region immediately adjacent to the membrane-spanning domain denominated as the pretransmembrane domain (PTM). The transmembrane region and cytoplasmic tail of SARS CoV S protein is only 52 amino acids long, which is the shortest length of all known coronavirus S proteins. Although the exact mechanism by which SARS-CoV enters the host cell has not been elucidated, it is most likely similar to other coronaviruses. Upon binding to the receptor at the host cell membrane, the fusion protein will be induced into the fusogenic intermediate state with a significant conformation change. This change is transmitted from S1 to S2, which causes the fusion peptide to be released from the interior of the protein and inserted into the target cell bilayer, exposing the S2 HR1 and HR2 regions. The fusion peptide is thought to be involved in clustering, orientation, and target membrane binding of trimeric spikes. This "metastable" fusion intermediate state is followed by a low-energy postfusion state that entails the formation of a six-helix bundle, in which HR1 helices fold into a central, coiled-coil

* To whom correspondence should be addressed. Tel: +34 966 658 762. Fax: +34 966 658 758. E-mail: jvillalain@umh.es.
[†] Universidad Miguel Hernández.
[‡] Instituto Superior Técnico.
[§] Faculdade de Ciências da Universidade de Lisboa.

10.1021/jp7118229 CCC: $40.75 
Published on Web 05/20/2008

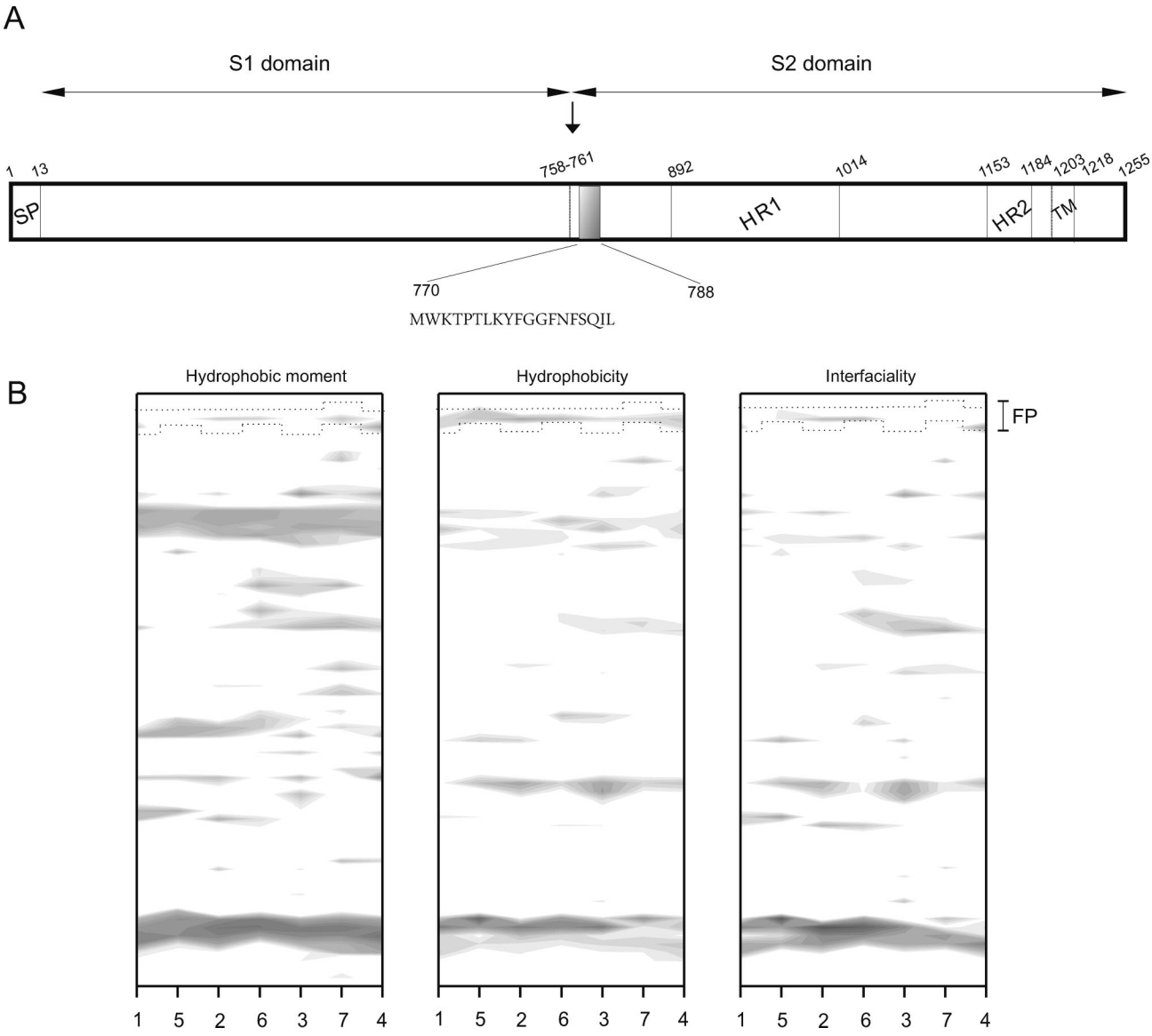


**Figure 1.** (A) Scheme of the structure of SARS-CoV spike glycoprotein S (amino acid residues 1−1255 for the full-length) as well as the S1 and S2 domains, according to literature consensus. The relevant functional regions are highlighted: the N-terminal signal peptide (SP), the transmembrane domain (TM), and the predicted heptad repeat regions pertaining to the S2 domain, HR1, and HR2. The putative fusion domain is located at the N terminus of the S2 subunit. The sequence of the peptide used in this work is also shown. It should be noted that the size of each domain is not drawn to an exact scale. (B) Hydrophobic moment, hydrophobicity, interfaciality distribution, and relative position of the $SARS_{FP}$ peptide along the SARS-CoV spike S2 domain used in this study, assuming it forms an α-helical wheel (see ref 36 for details). Only positive bilayer-to-water transfer free-energy values are depicted (shaded areas).

core in a parallel orientation and the three HR2 helices fold into an antiparallel orientation, packed onto the grooves of HR1 through hydrophobic interactions.[10,13–18] This fusion-active core structure brings the fusion peptide and transmembrane anchor together, driving the viral and target-cell membranes into close proximity, resulting in fusion between the membranes and formation of fusion pores, which allow the virus genome to enter the target cell.

Membrane fusion proteins share common motifs, with one of them being the "fusion peptide", a short segment of hydrophobic residues that is rich in Gly residues and essential for fusion. The fusion peptides interact with and insert into target membranes[19] because this region represents a surface patch with high bilayer-to-water transfer free-energy values (Figure 1B). Fusion peptides also participate in inducing lipid rearrangements, giving place to hemifusion and pore formation[20–22] and are also involved in pore enlargement. The fusion peptide does not function as an isolated unit, and in addition, it tends to self-associate in membranes in organized complexes in which several fusion peptide segments can act in a coordinated fashion. There are several pieces of evidence for the crucial role of fusion peptides in the fusion process. However, accurate information may be difficult to obtain from the complex system of an intact virus or a whole cell. Therefore, synthetic peptides corresponding to the putative fusion peptides may prove to be highly useful in determining structural characteristics to determine the way fusion peptides may interact with, penetrate into, and destabilize a lipid bilayer and study the influence of different lipid requirements on fusion by modulating the composition of the peptide-interacting membranes. Although much progress has been made in understanding the implication of fusion peptides of influenza, HIV, and other viruses in the membrane fusion process, available data concerning the fusion peptide of coronaviruses, particularly in the case of SARS-CoV, are scarce. In

the present work, we report on the determination of the secondary structure and the interaction with model membranes of a peptide pertaining to the fusion domain of SARS-CoV ($SARS_{FP}$). The structural and dynamical changes that take place in both the peptide and the phospholipid molecules induced by interaction with the lipid bilayer are characterized through a series of complementary experiments. Moreover, we show that $SARS_{FP}$ strongly partitions into phospholipids membranes and organizes differently in lipid environments, increasing the water penetration depth and displaying membrane activity modulated by the lipid composition of the membrane, suggesting that the $SARS_{FP}$ could be involved in the merging of the viral and target cell membranes.

**TABLE 1: Partition Coefficient ($K$p), Spectral Shift ($\Delta\lambda$), and Acrylamide Stern−Volmer ($K_{SV}$) Quenching Constant for the $SARS_{FP}$ Peptide in Buffer and in the Presence of LUVs of Different Compositions[a]**

| LUV composition | $K_p$ | $\Delta\lambda$ (nm) | $K_{sv}$ ($M^{-1}$) |
|---|---|---|---|
| EPC | nd | 3 | 7.90 |
| EPC/Chol 5:1 | nd | 3 | 10.7 |
| EPC/EPE/Chol 5:3:1 | nd | 2 | 10.0 |
| EPC/ESM/Chol 5:3:1 | nd | 0 | 11.6 |
| EPC/BPI/Chol 5:3:1 | $(0.80 \pm 0.25) \times 10^6$ | 7 | 4.40 |
| EPC/BPS/Chol 5:3:1 | $(1.60 \pm 0.43) \times 10^6$ | 7 | 3.60 |
| EPG | $(1.15 \pm 0.46) \times 10^6$ | 8 | 3.80 |
| $SARS_{FP}$ in buffer | | | 14.3 |

[a] $\Delta\lambda$ corresponds to a peptide/lipid ratio of 1:100.

## Experimental Methods

**Materials and Reagents.** A 19-residue peptide pertaining to the S2 domain of SARS-CoV ($^{770}$MWKTPTLKYFGGFNF-SQIL$^{788}$ with N-terminal acetylation and C-terminal amidation) was obtained from Genemed Synthesis, San Francisco, CA. The peptide was purified by reversed-phase HPLC (Vydac C-8 column, 250 × 4.6 mm; flow rate 1 mL/min; solvent A, 0.1% trifluoroacetic acid; solvent B, 99.9 acetonitrile and 0.1% trifluoroacetic acid) to better than 95% purity, and its composition and molecular mass were confirmed by amino acid analysis and mass spectroscopy. Because trifluoroacetate has a strong infrared absorbance at ~1673 $cm^{-1}$, which interferes with the characterization of the peptide amide I band,[23] residual trifluoroacetic acid, used both in peptide synthesis and in the high-performance liquid chromatography mobile phase, was removed by several lyophilization-solubilization cycles in 10 mM HCl. Egg phosphatidylcholine (EPC), egg phosphatidylglycerol (EPG), egg phosphatidic acid (EPA), egg sphingomyelin (ESM), bovine brain phosphatidylserine (BPS), egg trans-sterified phosphatidylethanolamine (EPE), bovine liver phosphatidylinositol (BPI), 1,2-dimyristoylphosphatidylcholine (DMPC), 1,2-dimyristoylphosphatidylglycerol (DMPG), 1,2-dimyristoylphosphatidylserine (DMPS), 1,2-dimyristoylphosphatidic acid (DMPA), Chol (Chol), *N*-lissamine rhodamine B 1,2-dihexadecanoyl-*sn*-glycero-3-phosphoethanolamine (RhB-PE), and *N*-(7-nitrobenz-2-oxa-1,3-diazol-4-yl)-1,2-dihexadecanoyl-*sn*-glycero-3-phosphoethanolamine (NBD-PE) were obtained from Avanti Polar Lipids (Alabaster, AL). 5-Carboxyfluorescein (CF) (>95% by HPLC), 5-doxylstearic acid (5NS), 16-doxylstearic acid (16NS), 4-(2-(6-(dioctylamino)-2-naphthalenyl)ethenyl)-1-(3-sulfopropyl)-pyridinium inner salt (di-8-ANEPPS), sodium dithionite, deuterium oxide (99.9% by atom), Triton X-100, EDTA, and HEPES were purchased from Sigma-Aldrich (Madrid, ES-EU). 8-Aminonaphthalene-1,3,6-trisulfonic acid (ANTS), *p*-xylene-bis-pyridinium bromide (DPX), and 1,6-diphenyl-1,3,5-hexatriene (DPH) were obtained from Molecular Probes (Eugene, OR). All other reagents used were of analytical grade from Merck (Darmstad, GER-EU). Water was deionized, twice-distilled, and passed through a Milli-Q apparatus (Millipore Ibérica, Madrid, ES-EU) to a resistivity higher than 18 MΩ cm.

**Liposome Preparation.** Liposomes were prepared as described previously.[24–26] The phospholipid and peptide concentrations were measured by methods described previously.[27,28]

**Leakage and Phospholipid-Mixing Measurements.** Phospholipid mixing was performed as described previously.[24–26]

**Kinetics of Leakage and Fusion.** The kinetics of leakage and fusion was analyzed from the parameters $L_{max}$ and $\tau$ (see Table 2) obtained by fitting an exponential function to the experimental time course curves. To obtain a good fitting, it was necessary to use a double exponential rate equation. Experimental leakage time course curves are described by the relationship $L = L_1(1 - \exp(-t/\tau_1)) + L_2(1 - \exp(-t/\tau_2))$, where $L_1$ and $L_2$ represent the maximum leakage, $t$ is the time after the addition of the peptide, and $\tau_1$ and $\tau_2$ are time constants. The average rate constants, $<\tau>$, were calculated according to $<\tau> = a_1\tau_1 + a_2\tau_2$, where $a_1$ and $a_2$ are the normalized fractional leakage component, $a_i = L_i/L_{max}$.

**Liposome Aggregation.** LUVs with a mean diameter of 0.2 $\mu$m were prepared in buffer containing 10 mM Tris, 0.1 M NaCl, and 1 mM EDTA. Peptide-induced vesicle aggregation was detected by monitoring the optical density at 405 nm on a 96-well Anthos spectrometer. All measurements were performed at room temperature on microtiter plates, with each well containing a final volume of 150 $\mu$L. The lipid concentration was 0.27 mM in all experiments, and the measured optical density was corrected for dilution upon peptide addition.

**Peptide Binding.** Peptide partitioning into membranes was evaluated by the enhancement of the tryptophan fluorescence by successive additions of small volumes of LUVs to the peptide sample ($3.2 \times 10^{-5}$ M peptide concentration). For details, see refs 24 and 25.

**Fluorescence Quenching of Trp Emission by Water-Soluble and Lipophilic Probes and Steady-State Fluorescence Anisotropy.** Fluorescence quenching and anisotropy studies were performed essentially as described previously.[24–26]

**Measurement of the Membrane Dipole Potential.** Aliquots containing the appropriate amount of lipid in chloroform−methanol (2:1, v/v) and di-8-ANEPPS were placed into a test tube to obtain a probe/lipid molar ratio of 1/100, and LUVs with a mean diameter of 0.1 $\mu$m were prepared as described previously. Steady-state fluorescence measurements were recorded with a Varian Cary Eclipse spectrofluorimeter. For details, see ref 26.

**Time-Resolved Fluorescence Spectroscopy.** Fluorescence intensity and anisotropy decays were obtained by the single-photon timing technique. For Trp, excitation was made at $\lambda$ = 295 nm with a dye laser of Rhodamine 6G.[29] For DPH excitation at 375 nm, a solid state Ti:sapphire laser was employed. The experimental layout is described in ref 30. The emission wavelength was 350 nm for Trp and 430 nm for DPH. The time scales ranged from 7.5 to 14.0 ps/channel for Trp and from 20.0 to 57.6 ps/channel for DPH (total time channels, 1024). The experimental fluorescence intensity and anisotropy decays were analyzed using the TRFA software (Scientific Software Technologies Center, Minsk, Belarus). For other details on the fluorescence intensity decay analysis and average fluorescence lifetime calculations, see refs 29 and 30. For other details on the time-resolved anisotropy measurements and analysis, see refs 31 and 32.

**TABLE 2: Fluorescence Lifetime Components $\tau_i$, Normalized Amplitudes $\alpha_i$, and Fluorescence Mean Lifetime (Amplitude-Weighted, $\bar{\tau}$, and Intensity-Weighted, $<\tau>$) of the Trp Residue of the $SARS_{FP}$ Peptide in Buffer and in the Presence of Some Phospholipid Model Membranes at 25 °C, and the Reduced $\chi^2$ Values of the Fits to the Experimental Fluorescence Decays**

| system | $\tau_1$ (ns) | $\tau_3$ (ns) | $\tau_3$ (ns) | $\alpha_1$ | $\alpha_2$ | $\alpha_3$ | $\bar{\tau}$ (ns) | $<\tau>$ (ns) | $\chi^2$ |
|---|---|---|---|---|---|---|---|---|---|
| buffer 15 °C | 0.395 | 1.43 | 3.15 | 0.368 | 0.394 | 0.238 | 1.46 | 2.21 | 1.10 |
| buffer 25 °C | 0.301 | 1.32 | 3.31 | 0.310 | 0.498 | 0.192 | 1.39 | 2.17 | 1.23 |
| buffer 50 °C | 0.179 | 0.824 | 2.16 | 0.310 | 0.563 | 0.126 | 0.79 | 1.24 | 1.12 |
| EPC | 0.444 | 1.56 | 4.20 | 0.350 | 0.485 | 0.165 | 1.60 | 2.59 | 1.16 |
| EPG | 0.391 | 1.47 | 3.70 | 0.320 | 0.449 | 0.231 | 1.64 | 2.55 | 1.28 |
| EPC/Chol5:1 | 0.332 | 1.35 | 4.20 | 0.475 | 0.388 | 0.137 | 1.26 | 2.52 | 1.15 |
| EPC/BPS/Chol5:3:1 | 0.360 | 1.42 | 3.62 | 0.335 | 0.480 | 0.185 | 1.47 | 2.34 | 1.17 |

**Infrared Spectroscopy.** Aliquots containing the appropriate amount of lipid in chloroform/methanol (2:1, v/v) were placed in a test tube containing 200 $\mu$g of dried lyophilized peptide. After vortexing, the solvents were removed by evaporation under a stream of $O_2$-free nitrogen, and finally, traces of solvents were eliminated under vacuum in the dark for more than 3 h. The samples were hydrated in 200 $\mu$L of $D_2O$ buffer containing 20 mM HEPES, 50 mM NaCl, and 0.1 mM EDTA with pH 7.4 and incubated at 10 °C above the phase transition temperature ($T_m$) of the phospholipid mixture with intermittent vortexing for 45 min to hydrate the samples and obtain multilamellar vesicles (MLV). The spectra were obtained and analyzed as described previously.[33,34]

## Results

The SARS-CoV spike glycoprotein consists of an extracellular domain, a TM domain, and an intracellular domain (Figure 1A), and it can be classified as a class I viral fusion protein. It is also known that apart from the FP, other regions of viral fusion proteins bind and interact with membranes and experience conformational changes that altogether combine to make possible the fusion of the viral and cell membranes.[19,35] Recently, we have shown the existence of different membranotropic regions of the SARS spike glycoprotein by using a library of 16-/18-mer peptides encompassing the full sequence of the protein,[36] which might be important not only for modulating membrane binding and interaction but also for protein–protein interaction. To detect surfaces along the SARS spike glycoprotein that might be identified as membrane partitioning or membrane interacting-ability zones, we have plotted the average surface hydrophobic moment, hydrophobicity, and interfaciality versus the amino acid sequence, supposing it adopts an α-helical structure along the whole sequence, giving us a depiction of the potential surface zones that could be possibly implicated in membranotropic action (Figure 1B; see also ref 36). These patches of positive hydrophobicity and interfaciality along the surface of the protein could favor the interaction with other similar patches along the same or other proteins as well as with the surface of the membrane. One of these membranotropic regions (Figure 1) has been proposed to be the putative fusion peptide of the SARS spike glycoprotein, $SARS_{FP}$. Because $SARS_{FP}$ could be important in the membrane fusion process, we present here the results of the study of the interaction of $SARS_{FP}$ with model membranes.

**$SARS_{FP}$ Membrane Binding and Interaction.** The intensity of the fluorescence emission of a Trp residue increases when the amino acid is in a hydrophobic environment, such as a phospholipid membrane, and together with an increase in the quantum yield, the maximal spectral position shifts toward shorter wavelengths.[34] The increase in fluorescence emission intensity of the Trp residue of the $SARS_{FP}$ peptide as a function of the increasing lipid concentration is shown in Figure 2A. From data fitting, partition coefficients, $K_p$, were obtained for the different phospholipid compositions (summarized in Table 1). Large $K_p$ values (in the range $10^6$) were obtained for negatively charged phospholipids-containing bilayers, even at increasing ionic strengths (Figure 2A), showing that the peptide has a strong preference for the membrane, as compared to the aqueous environment. These results were further corroborated by the displacement in the emission frequency maximum of

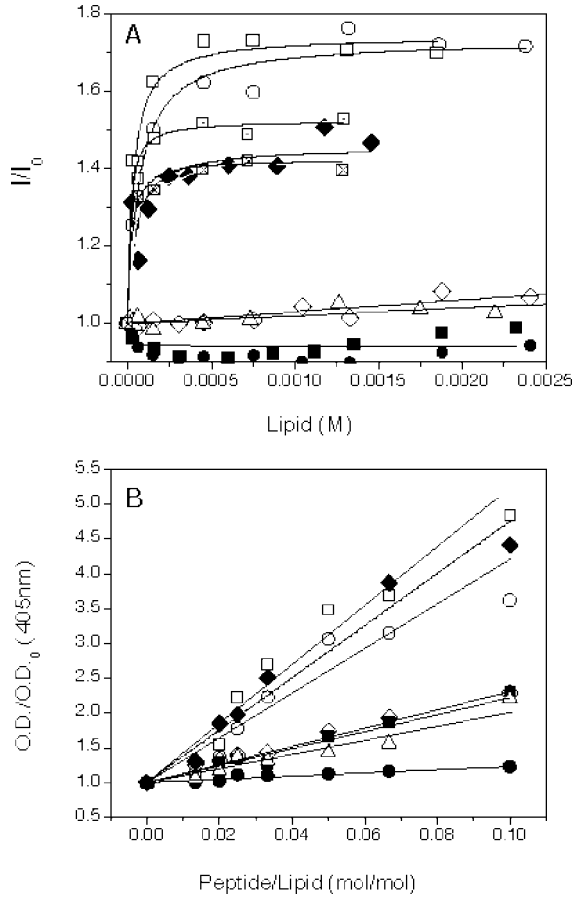


**Figure 2.** (A) Change on the tryptophan fluorescence intensity of the $SARS_{FP}$ peptide in the presence of increasing lipid concentration with the fit to the data and (B) variation of optical density (monitoring of LUV aggregation) for different lipid compositions at different peptide-to-lipid ratios (lines are only to guide the eye). The lipid compositions used were EPG (♦), EPC (■), EPC/BPI/CHOL (5:3:1) (○), EPC/BPS/CHOL (5:3:1) (□), EPC/EPE/CHOL (5:3:1) (△), EPC/ESM/CHOL (5:3:1) (●), and EPC/CHOL (5:1) (◊). In panel A, the tryptophan fluorescence intensity of the $SARS_{FP}$ peptide was measured also in LUVs composed of EPC/BPS/CHOL (5:3:1) in buffer containing 100 mM NaCl (⊡) and 150 mM NaCl (square with ×).

Trp in the presence of phospholipid LUVs. In the case of the $SARS_{FP}$ peptide, the maximum of the fluorescence emission spectra decreased up to 7–8 nm upon addition of negatively charged vesicles and 0–3 nm when the peptide was titrated with neutral vesicles (Table 1), suggesting a more hydrophobic (low-polarity) environment surrounding the tryptophan residue in the presence of negatively charged phospholipids than in the presence of zwitterionic phospholipids. Interstingly, for EPC and /EPC/ESM containing liposomes, a slight decrease in fluorescence intensity was observed (Figure 2A). This nontrivial effect will be rationalized in the Discussion. Because membrane apposition is a necessary requisite before membrane fusion can occur,[37] the ability of the $SARS_{FP}$ peptide to induce vesicle aggregation was tested to investigate whether this property correlated with the peptide−membrane binding and leakage assays. The ability of the peptide to induce vesicle aggregation was monitored through the increment in optical density as a function of the peptide/lipid ratio, as shown in Figure 2B. It can be observed that the effect of the $SARS_{FP}$ peptide is larger in liposomes containing negatively charged phospholipids than on zwitterionic ones, in a similar way to the fluorescence data shown above. The $SARS_{FP}$ peptide has a positive net formal charge of +2, so an electrostatic effect might be the reason that high $K_p$ values and also significant vesicle aggregation for compositions containing negatively charged phospholipids are observed. However, it is not only the electrostatic attraction that is playing a role, because an increase in the ionic strength does not decrease the partition coefficient, which it would in the case of a purely electrostatic interaction. In addition to electrostatic effects, hydrophobic interactions also play an important role, which is relevant because the outer leaflet of the target membrane for the virus is mainly zwitterionic.

Another way of evaluating the interaction of the peptide with the membrane is by determining the fluorescence intensity decay of the Trp residue. The decay of Trp is usually complex, since more than two exponentials are required for a good description, and from this complexity, subtle alterations undergone by the peptide upon membrane insertion can be detected. In Table 2, the parameters describing the $SARS_{FP}$ fluorescence decay, the lifetime-weighted quantum yield, and the average fluorescence lifetime are shown in buffer at different temperatures and in the presence of different lipid mixtures at 25 °C. In all systems, the fluorescence decay was described by the sum of three exponentials with lifetime components typical of Trp-containing peptides. In buffer and as expected, the lifetime decreases with increasing temperature, because the nonradiative decay processes become more effective. However, from 25 to 15 °C, there are changes in the sequence of pre-exponentials (not verified between 25 and 50 °C), whereas the lifetime-weighted quantum yield and mean lifetime show very modest changes, suggesting the existence of a structural alteration between 15 and 25 °C. In the presence of different lipid mixtures, there are small but appreciable changes in the lifetime parameters. In general, the lifetime-weighted quantum yield is increased as compared to the value in buffer at the same temperature, except for the EPC/Chol system. In the case of pure lipid vesicles (EPC and EPG) and in the EPC/BPS/Chol mixture, the normalized pre-exponentials show no drastic changes relative to the fluorescence decay in water at 25 °C, suggesting that there are no strong structural alterations of the peptide in the vicinity of the Trp residue upon membrane incorporation. In the case of the EPC/Chol mixture, the changes are more pronounced; namely, the pre-exponential of the long component is significantly reduced with a concomitant increase in the pre-exponential of the short

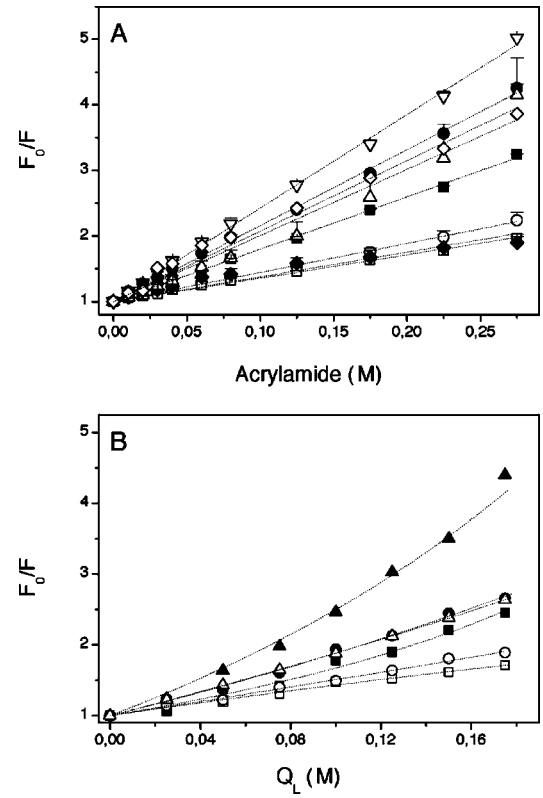


**Figure 3.** (A) Stern−Volmer plots of the quenching of the Trp fluorescence emission of $SARS_{FP}$ by acrylamide in aqueous buffer (▽) and in the presence of liposomes composed of EPG (♦), EPC (■), EPC/BPI/CHOL (5:3:1) (○), EPC/BPS/CHOL (5:3:1) (□), EPC/EPE/CHOL (5:3:1) (△), EPC/SM/CHOL (5:3:1) (●), and EPC/CHOL (◊) and fitting of the Stern−Volmer equation. (B) Quenching of the Trp fluorescence emission of $SARS_{FP}$ by 5NS (solid symbols) and 16NS (open symbols) in LUVs composed of EPC (■, □), EPC/BPS/CHOL at a molar ratio of 5:3:1 (●, ○) and EPG (▲, △) vs the effective quencher concentration. The lipid-to-peptide ratio was 50:1.

one. In all other cases, it is obvious that the changes observed in the lifetime-weighted quantum yield do not correlate with those of the steady-state fluorescence intensity (whereas the former increases between ∼5 and 20%, depending on the system, the latter decreases ∼10% in EPC and increases ∼45% for EPG and ∼60% for EPC/BPS/Chol). Taken together, this can be interpreted by the existence in water of a second population of peptide that does not fluoresce (probably due to the intraquenching effect of the Lys residues of the peptide or to aggregate formation); in the case of anionic membranes, when the peptide partitions into the membrane, there is a structural alteration to a species with a higher quantum yield, and this effect adds up to the relief of the quenching. As previously described, this is not the case for the zwitterionic membranes.

**Studies of the Penetration and Location of $SARS_{FP}$ in the Bilayer.** To further explore the possible interaction of $SARS_{FP}$ with the lipid bilayer, we studied the accessibility of its Trp residue toward acrylamide, a neutral, water-soluble, highly efficient quencher that is unable to penetrate into the hydrophobic core of the lipid bilayer. The quenching data is presented in Figure 3A, and the resultant Stern−Volmer plots (Table 1) reveal a lesser decrement in fluorescence intensity in the presence of liposomes so that the Trp residue was less accessible to the quencher in the presence of LUVs. In addition, the smallest $K_{SV}$ values were obtained in the presence of negatively charged phospholipids, EPG, EPC/BPS/CHOL, and EPC/BPI/

**TABLE 3: Fluorescence Lifetime Components $\tau_i$, Normalized Amplitudes $\alpha_i$, and Fluorescence Mean Lifetimes (Amplitude-Weighted, $\bar{\tau}$, and Intensity-Weighted, $<\tau>$) of DPH in Phospholipid Model Membranes in the Absence and in the Presence of the $SARS_{FP}$ Peptide below and above the Phospholipid $T_m$**

| $T$ (°C) | system | $\tau_1$ (ns) | $\tau_3$ (ns) | $\tau_3$ (ns) | $\alpha_1$ | $\alpha_2$ | $\alpha_3$ | $\bar{\tau}$ (ns) | $<\tau>$ (ns) | $\chi^2$ |
|---|---|---|---|---|---|---|---|---|---|---|
| 15 °C | DMPG + $SARS_{FP}$ | 0.455 | 2.05 | 8.41 | 0.318 | 0.458 | 0.224 | 2.97 | 6.01 | 1.15 |
| | DMPG | 0.876 | 6.17 | 12.17 | 0.136 | 0.085 | 0.778 | 10.12 | 11.72 | 1.24 |
| | DMPC + $SARS_{FP}$ | 0.779 | 3.13 | 9.17 | 0.205 | 0.520 | 0.275 | 4.30 | 6.57 | 1.09 |
| | DMPC | | 6.11 | 9.85 | 0 | 0.245 | 0.755 | 8.93 | 9.22 | 1.07 |
| 35 °C | DMPG + $SARS_{FP}$ | 0.290 | 1.67 | 6.40 | 0.360 | 0.511 | 0.129 | 1.78 | 3.78 | 1.12 |
| | DMPG | | 1.50 | 9.19 | 0 | 0.182 | 0.818 | 7.79 | 8.92 | 1.06 |
| | DMPC + $SARS_{FP}$ | 0.502 | 2.591 | 7.487 | 0.128 | 0.472 | 0.400 | 4.28 | 5.98 | 1.12 |
| | DMPC | | 2.830 | 7.947 | 0 | 0.137 | 0.823 | 7.24 | 7.67 | 1.09 |

CHOL. Interestingly, the $K_{SV}$ value for Chol-containing zwitterionic membranes was only slightly smaller than in the absence of liposomes, and for EPC LUVs, the $K_{SV}$ value is between both types of membrane compositions. The plots are linear with a unitary intercept, showing that the Stern−Volmer dynamic quenching formalism accurately describes the data. The $K_{SV}$ value is actually the product of the bimolecular quenching rate constant times the average fluorescence lifetime of the fluorophore in the absence of quenching. In this way, it is important to check if there are significant variations in that parameter to compare quencher accessibility from $K_{SV}$ values. At 25 °C, the average lifetime values (Table 2) lie always between 2.17 and 2.59 ns, and in general, the systems for which a larger $K_{SV}$ was retrieved corresponded to a shorter average lifetime: the order of $K_{SV}/<\tau>$ is the same as $K_{SV}$ alone, except for EPG and EPC/BPS/Chol, which switch but remain very similar. Therefore and after accounting for the mean lifetime variations, the accessibility to the aqueous quencher becomes fully correlated with the spectral shifts observed. The transverse location (penetration) of the $SARS_{FP}$ peptide into the lipid bilayer was evaluated by monitoring the relative quenching of the fluorescence of the Trp residues by the lipophilic spin probes 5NS and 16NS when the peptide was incorporated into the fluid phase of vesicles having different phospholipid compositions (Figure 3B). It can be seen that in general and for each one of the different membrane compositions studied, the $SARS_{FP}$ peptide was quenched more efficiently by 5NS, quencher for molecules near or at the interface, than by 16NS, quencher for molecules buried deeply in the membrane, allowing one to conclude that $SARS_{FP}$ remained close to the lipid/water interface.

**Fluorescence Lifetime of DPH Incorporated into the Membrane.** The effect of the $SARS_{FP}$ peptide on the chain-packing order and structural and thermotropic properties of phospholipid membranes was further investigated by measuring the fluorescence decay of DPH, which is known to partition mainly into the hydrophobic core of the membrane. The fluorescence intensity decay of a membrane probe such as DPH is one of the most sensitive parameters for evaluating perturbations that might take place in the interior of the lipid bilayer. The amplitude and lifetime values of the fluorescence decay components, as well as the values of lifetime-weighted quantum yield and average lifetime of DPH incorporated either in a zwitterionic (DMPC) or an anionic (DMPG) membrane, both below and above the $T_m$ of the phospholipid and in the absence and in the presence of $SARS_{FP}$, are given in Table 3. In the absence of the peptide, the fluorescence decay of DPH is always biexponential, except for DMPG at 15 °C, where a longer component of ~12 ns is the major one, giving rise to a longer lifetime-weighted quantum yield and average lifetime. The presence of the $SARS_{FP}$ peptide makes the decay more complex, originating a short (subnanosecond) component with an amplitude of more than ~13−36%. The other components become significantly shorter for DMPG, but this is not the case for DMPC. In addition, in the case of DMPC, the quantum yield and the average lifetime are almost independent of temperature. In the case of DMPG, the short component is shorter and contributes more to the decay, and the average lifetime becomes distinctly smaller than in all other cases. Thus, the relative decrease in the average lifetime is stronger for DMPG both above and below $T_m$.

**Membrane Rupture, Phospholipid Mixing, and Fusion.** To explore the effect of $SARS_{FP}$ in the destabilization of membrane vesicles, we studied its effect on the release of encapsulated fluorophores in model membranes made up of various compositions at different peptide-to-lipid molar ratios (Figure 4A, C). LUVs were composed of unsaturated phospholipids instead of saturated ones to avoid the great variability in the basal fluorescence and the rapid release of the probes even in the absence of the peptide as reported previously.[34] The final maximum values ($L_{max}$), the rate constants ($\tau$), and the average rate constant $<\tau>$ of the processes obtained from Figure 4A are summarized in Table 4 (see Experimental Methods). Considering the average rate constant as the relevant parameter for intersystem comparison, the lower ones, that is, the faster leakage elicited by $SARS_{FP}$, took place in LUVs composed of EPC/BPI/Chol, followed by LUVs composed of EPC/BPS/Chol, EPC/Chol, and EPC (Table 4). The extent of leakage observed at different $P/L$ ratios and the effect of lipid composition is shown in Figure 4C, where it can be seen that the peptide was able to induce the release of the internal contents of the liposomes in a dose-dependent manner. In the presence of liposomes composed of either EPC/BPI/CHOL or EPC/BPS/CHOL, the $SARS_{FP}$ peptide induced a high percentage of leakage (leakage values of ~95% at a lipid/peptide ratio of 10:1). Slightly lower leakage values were obtained for liposomes composed of EPC/SM/CHOL, EPC, or EPC/CHOL (leakage values of between 80 and 90% at a lipid/peptide ratio of 10:1), whereas LUVs composed of EPC/EPE/CHOL, EPG, and EPA displayed much lower leakage values (between 55 and 70% at a lipid/peptide ratio of 10:1). This shows that all these membranes are perturbed by the peptide, in agreement with the effect observed on the DPH fluorescence lifetime.

The induction of inner-monolayer phospholipid mixing by the $SARS_{FP}$ peptide, as a measure of its fusogenic activity, was tested with several types of vesicles utilizing the probe dilution assay[38,39] (Figure 4B, D). It became evident that the $SARS_{FP}$ peptide could induce significant inner-monolayer lipid mixing only in the presence of liposomes composed of negatively charged phospholipids but not with zwitterionic ones. Considering the average rate constant as before, the lower ones, that is, the faster mixing, took place in LUVs composed of EPC/BPI/Chol, EPC/BPS/Chol, and EPG, but much lower on the other compositions tested (Table 4). This can be confirmed by observing the extent of mixing in Figure 4D, where only relevant

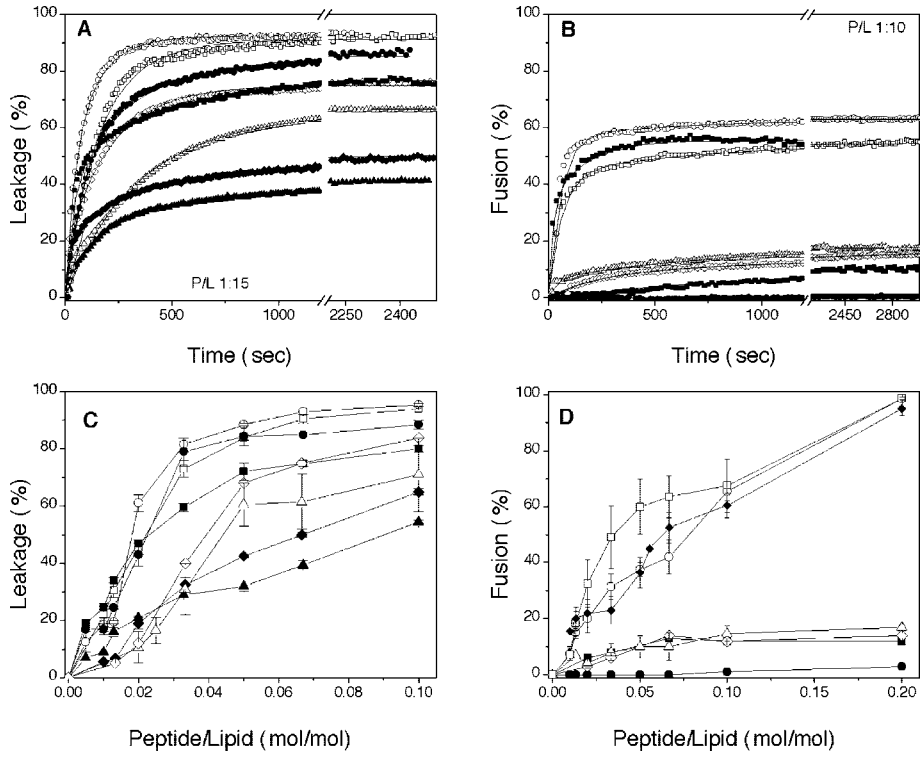


**Figure 4.** Effect of the $SARS_{FP}$ peptide on membrane rupture (that is, leakage (A, C)) and membrane phospholipid mixing of the inner monolayer (that is, fusion (B, D)) of fluorescent probes encapsulated in LUVs of different lipid compositions at different lipid-to-peptide molar ratios. The kinetic and extent assays are shown in panels A and B and in panels C and D, respectively. The lipid compositions were EPC (■), EPG (♦), EPA (▲), EPC/BPI/CHOL (5:3:1) (○), EPC/BPS/CHOL (5:3:1) (□), EPC/EPE/CHOL (5:3:1) (△), EPC/SM/CHOL (5:3:1) (●), and EPC/CHOL (5:1) (◊). See text for details and Table 4 for the fitting parameters.

**TABLE 4: Fitted Parameters for Leakage and Fusion Induced by $SARS_{FP}$ in LUVs of Different Lipid Compositions**[a,b]

| LUV composition | leakage (% $L_{max}$) | $\tau_1$ (s) | $\tau_2$ (s) | $<\tau>$ (s) | fusion (% $F_{max}$) | $\tau_1$ (s) | $\tau_2$ (s) | $<\tau>$ (s) |
|---|---|---|---|---|---|---|---|---|
| EPC | 77 | 38 | 406 | 196 | 10 | 1523 | 1548 | 1531 |
| EPG | 50 | 65 | 1000 | 425 | n.d. | n.d. | n.d. | n.d. |
| EPA | 41 | 98 | 682 | 369 | n.d. | n.d. | n.d. | n.d. |
| EPC/Chol5:1 | 75 | 210 | 13 | 168 | 15 | 2489 | 223 | 1482 |
| EPC/EPE/Chol5:3:1 | 66 | 546 | 239 | 395 | 18 | 737 | 31 | 502 |
| EPC/SM/Chol5:3:1 | 85 | 76 | 346 | 203 | 1 | | | |
| EPC/BPI/Chol5:3:1 | 92 | 43 | 138 | 91 | 63 | 57 | 680 | 125 |
| EPC/BPS/Chol5:3:1 | 91 | 120 | 212 | 165 | 63 | 60 | 625 | 186 |

[a] The lipid to peptide ration was 15:1 for leakage and 10:1 for fusion. [b] See Figure 4 for experimental data and fitting curves.

values are observed for compositions having negatively charged phospholipids (~100% for inner-monolayer phospholipid mixing but discrete for the other compositions). Significantly, although fusion is similar for all vesicles containing negatively charged phospholipids, leakage is lower for pure anionic vesicles (compare Figure 4C, D), suggesting that the $SARS_{FP}$ peptide induces nonleaky fusion, which is more relevant in virus-membrane fusion processes. In fact, this is true at high lipid-to-peptide ratios as observed by contents mixing using ANTS/DPX[40] (not shown for briefness), which are usually closer to the in vivo conditions.

**Modulation of Membrane Dipole Potential.** Changes in the membrane dipole potential magnitude elicited by $SARS_{FP}$ was monitored by means of the spectral shift of the fluorescence probe di-8-ANEPPS.[41–43] Furthermore, to confirm the specific effect of the $SARS_{FP}$ peptide on liposomes containing negatively charged phospholipids, we chose LUVs containing only one phospholipid plus cholesterol. The variation of the fluorescence intensity ratio $R_{450/520}$ normalized as a function of the peptide concentration for different membrane compositions is shown in Figure 5. In the presence of the peptide, a great decrease in the $R_{450/520}$ value was measured only in the presence of negatively charged lipid mixtures, that is, those containing either BPS, EPA, or EPG/Chol, confirming again the specific interaction of the peptide with vesicles bearing negatively charged phospholipids.

**Peptide Secondary Structure from FTIR.** The existence of structural changes on the $SARS_{FP}$ peptide induced by membrane binding was studied by Fourier transformed infrared spectroscopy (FTIR). Self-deconvolution, derivation, and band-fitting was applied to the original envelope to observe the underlying components of the broad amide I′ band between 1700 and 1600 $cm^{-1}$[24] at 10 °C above the phospholipid $T_m$, that is, in the fluid state, and 30 °C for the peptide in solution. For the peptide in solution, band-fitting yielded different component bands at frequencies about 1672, 1657, 1643, 1630, and 1618 $cm^{-1}$ (not shown for briefness) that can be respectively assigned to $\beta$-turns, α-helix, or $3_{10}$-helix, unordered structures, $\beta$-sheet, and extended $\beta$-strands with strong intermolecular interactions, respectively.[24] The frequencies of the amide I′ component bands for $SARS_{FP}$ in the presence of DMPC, DMPG, and DMPA were nearly identical to those found for the peptide in solution, but

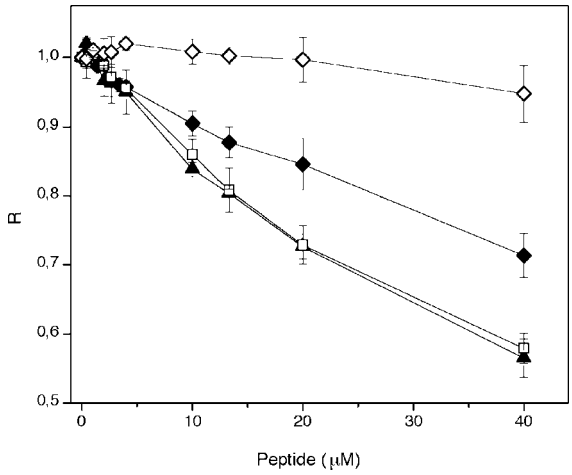


**Figure 5.** Effect of the $SARS_{FP}$ peptide on the membrane dipole potential monitored through the fluorescence ratio ($R$) of di-8-ANEPPS-labeled LUVs containing different lipid compositions at different lipid-to-peptide molar ratios. The lipid compositions were EPC/CHOL (5:1) (◊), EPG/CHOL (5:1) (♦), EPA/CHOL (5:1) (▲), and BPS/CHOL (5:1) (□).

their intensity varied slightly (not shown for briefness). The most significant difference between the peptide amide I′ band in the different systems studied is the increase in the relative intensity of the bands assigned to extended $\beta$-strands with strong intermolecular interactions in the presence of the phospholipids (from 31 to ∼35–36%), as well as an increase in half-bandwidth at half-height of ∼3–8 $cm^{-1}$ (not shown). A significant part of the structure is retained in all cases, in agreement with the fluorescence intensity decay parameters of the peptide, which show absence of strong alterations around the Trp residue (see below).

**Fluorescence Anisotropy of the Trp Residue of $SARS_{FP}$.** Another relevant fluorescence parameter is the steady-state fluorescence anisotropy of the Trp residue of $SARS_{FP}$, which gives insight on the motional restrictions affecting the Trp region of the peptide when inserted into the membrane. However, the anisotropy is also very sensitive to the size of the entity containing the fluorophore, especially in solution, where the viscosity is low enough to make the rotational diffusion to take place in the time scale of the fluorescence emission. Thus, it helps to determine the aggregation state of the peptide in water, because the size of the particle is directly proportional to the number of molecules in the aggregate. One simple way of obtaining this information is from the rotational correlation time $\phi$ of the peptide in buffer solution, which can be retrieved from the fluorescence anisotropy decay. This parameter can be predicted from simple calculations assuming a spherical rotor (Stokes–Einstein equation): $\phi = \eta V/RT$, where $\eta$ is the solvent's viscosity, $V$ is the hydrodynamic volume of the peptide, $R$ is the gas constant, and $T$ is the absolute temperature. The volume of the peptide can be calculated from the amino acid sequence,[44] giving a value of 2812 $Å^3$. The input value of $V$ can be doubled, tripled, etc. to retrieve the expected value of $\phi$ for a dimer, a trimer, etc. The value of $\phi$ can be also obtained experimentally from the fluorescence anisotropy decay (not shown; see Experimental Methods). In Table 5, the experimental value of $\phi$ together with the values predicted for a monomer and a dimer (Stokes–Einstein equation) are given for 15 and 25 °C. It can be easily observed that the experimental value is much closer to the monomer value, even slightly shorter. To further confirm that the value of $\phi$ obtained from the fit to the experimental anisotropy decay is correct (because this is a complex mathematical procedure), the steady-state anisotropy was also calculated from the Perrin equation, that is, $\langle r \rangle = r_0/(1 + \langle \tau \rangle/\varphi)$, where $r_0$ is the fundamental anisotropy (these values are also shown in Table 5). The original equation is valid for a fluorophore with a monoexponential decay, but we have previously verified that this simplified form with the mean fluorescence lifetime is a very good approximation for Trp-containing peptides in buffer solution.[32] The agreement between the experimental steady-state anisotropy and the anisotropy calculated from the Perrin equation with the experimental $\phi$ is very good, and it can be safely concluded that the fluorescent peptide species is largely monomeric in water in the concentration and temperature range used for fluorescence experiments. Upon interaction with the membrane, the anisotropy significantly changes. In the case of the zwitterionic mixture, there is a slight increase of the anisotropy, whereas for the anionic membranes, there is a larger increase. It is usual to observe an increase in the anisotropy of Trp for peptides interacting with the membrane because the movements of both the indol ring and the peptide backbone are slower and more restricted. The effect correlates with previous parameters described in this work that account for the strength of the interaction of the peptide with those membranes.

**TABLE 5: Rotational Correlation Time, $\phi$, of the Peptide in Buffer Solution at Different Temperatures and Steady-State Anisotropy $<r>$ of the Peptide in the Absence and in the Presence of Different Lipid Membranes at 25 °C**

| system | $<r>_{experimental}$ | $<r>_{integration}$[a] | $\phi_{experimental}$ (ns)[b] | $\phi_{monomer}$ (ns)[c] | $\phi_{dimer}$ (ns)[c] |
|---|---|---|---|---|---|
| buffer 15 °C | 0.059 | 0.062 | 0.71 | 0.81 | 1.61 |
| buffer 25 °C | 0.053 | 0.052 | 0.57 | 0.61 | 1.22 |
| EPC/Chol 5:1 | 0.066 | | | | |
| EPG | 0.139 | | | | |
| EPC/BPS/Chol 5:3:1 | 0.103 | | | | |

[a] From Perrin equation using the experimental $\phi$. [b] From the fit of a monoexponential decay law to the experimental fluorescence anisotropy decay curve (not shown). [c] From the Stokes–Einstein equation.

## Discussion

Membrane fusion can be described as a succession of different steps; namely, apposition of membranes; hemifusion of the outer leaflets to form a stalk; fusion pore formation through merging of both bilayers at the stalk point; and finally, fusion pore enlargement with full contents mixing.[45,46] The membrane fusion protein of SARS CoV is the envelope Spike glycoprotein, and it is thought that several trimers of the S protein are capable of juxtaposing, destabilizing, and merging the viral and cellular membranes so that a fusion pore is formed as has been already described for other class I membrane fusion proteins. Furthermore, there are several regions within class I and class II membrane fusion proteins that are involved in the fusion process and are decisive for membrane fusion to take place because destabilization of the lipid bilayer and membrane fusion appears then to be the result of the binding and interaction of these segments with the biological membranes. We have selected a specific segment from the SARS CoV sequence that is proposed to be the putative fusion peptide of the SARS spike glycoprotein[36] to carry out a biophysical study, aiming to elucidate how the capacity of this region to interact and disrupt membranes depends on lipid composition and which structural and dynamic features are relevant for that disruption.

The SARS-CoV $SARS_{FP}$ peptide studied in this work partitions with high affinity to model membranes having different phospholipid compositions. The degree of partitioning of the SARS-CoV $SARS_{FP}$ peptide is much higher for vesicles containing negatively charged phospholipids, as it has also been found for other peptides pertaining to other membrane fusion proteins, which showed similar binding affinities, as reported previously.[24,25,47] This specificity was further demonstrated by the ability of the $SARS_{FP}$ peptide to induce vesicle aggregation because it was greater on liposomes containing negatively charged phospholipids than on zwitterionic ones. The binding force was mainly from an electrostatic origin, presumably owing to the positive net charge (+2) of the peptide. However, hydrophobic interactions also play an important role because the parameters described above do not completely correlate to the total surface charge of the different membranes used. This is the case of the mixtures containing 33% BPS or BPI. Not only the headgroup is different, but also a contribution arising from the fact that *sn*-1/*sn*-2 acyl chains are mainly saturated/monounsaturated in BPS and saturated/polyunsaturated in PI cannot be ruled out.

As pointed out previously, for EPC and EPC/ESM-containing liposomes, a slight decrease in fluorescence intensity was observed (Figure 2A). This nontrivial effect can be due either to a structural alteration where the Lys residues that would make it become more accessible to the Trp, thereby quenching its emission (see ref 48), or to the formation of aggregates with a concomitant quenching of Trp emission. This was further demonstrated by hydrophilic (acrylamide) and lipophilic (NS) probe quenching. In the case of acrylamide quenching data, the smallest $K_{SV}$ values were observed in the presence of negatively charged phospholipids, suggesting that the $SARS_{FP}$ Trp residue is less accessible for quenching by acrylamide and therefore interacting more deeply with the membrane. However, it was also shown above that the $SARS_{FP}$ peptide was quenched more efficiently by 5NS than by 16NS, suggesting that in all cases, the peptide was near the membrane lipid/water interface in a shallow position. A greater quenching efficiency was observed for model membranes containing only negatively charged phospholipids, suggesting that in the case of EPC/BPS/Chol, the Trp residue is somehow less accessible to both lipophilic probes than in EPG, probably because it is in an aggregate form relevant for its biological action (note that the Trp in the case of EPC/BPS/Chol is also less accessible to the aqueous quencher acrylamide). This suggests that the organization of the peptide in the membrane is not the same in EPG and EPC/BPS/Chol, because the quenching efficiency is higher with both 5NS and 16NS for the EPG case. This is in agreement with a different membrane/water steady-state intensity ratio and lifetime-weighted quantum yield observed for the peptide in these two anionic systems. This was confirmed by the longer fluorescence decay lifetimes of the Trp residue of the peptide in the presence of either one anionic or one zwitterionic lipid (EPG or EPC), as compared to the anionic or zwitterionic mixture, respectively (EPC/BPS/Chol and EPC/Chol). This reduction in lifetime could be a consequence of a self-quenching process effective in regions that are peptide-enriched.

The SARS-CoV $SARS_{FP}$ peptide was also capable of altering membrane stability, causing the release of fluorescent probes. However, this effect was dependent on lipid composition and on the lipid/peptide molar ratio, being the highest effect observed for liposomes containing negatively charged phospholipids. Lower but significant leakage values were also observed for liposomes composed of zwitterionic phospholipids so that the effect observed on these vesicles should be due primarily to hydrophobic interactions within the bilayer but not to the specific charge of the phospholipid head-groups. In fact, all the data shows that although the peptide is able to interact and perturb the zwitterionic membranes, the strength of the interaction is insufficient to induce extensive fusion; that is, the aggregation activity of the peptide is quite limited with those membranes. For example, the fluorescence decay of DPH was affected by the peptide both in DMPC and in DMPG membranes, although the perturbation was stronger with the latter lipid. The short component and the shortening of the other components in DPH fluorescence decay induced by the peptide (Table 3) may be interpreted as a deeper penetration of water into the acyl chain region, because it is well-known that the quantum yield of DPH is quite low in water. Thus, in the case of DMPG, all the bilayer is strongly and deeply perturbed. On the other hand, in the case of DMPC, there is a similar membrane perturbation with water penetration revealed by the short component, but the perturbation is not as strong as in the case of DMPG because the average lifetimes do not decrease so drastically. Thus, the water penetration and membrane perturbation sensed by DPH relates with the membrane activity essays of leakage and fusion.

The binding to the surface and the modulation of the phospholipid biophysical properties that take place when the peptide is bound to the membrane (that is, partitioning into the membrane surface and perturbation of the bilayer architecture) could be related to the conformational changes that might occur during the activity of the SARS-CoV spike protein. In the case of zwitterionic membranes, it is probable that the adequate conformational changes are not taking place. The induction of fusion by the $SARS_{FP}$ peptide was also studied, and similar results were obtained because specific and large membrane fusion values were found only in the presence of liposomes composed of negatively charged phospholipids. These data were confirmed by the change in the membrane dipole potential elicited by $SARS_{FP}$ in the presence of vesicles bearing negatively charged phospholipids. The differences we have found on the effect produced by the $SARS_{FP}$ peptide on leakage and fusion (that is, high values in the presence of negatively charged phospholipids but lower for the other types of phospholipids studied here) might indicate that negatively charged phospholipids could play an important role and stimulate the fusion process. That is, approximation and binding of the protein to the membrane occurs for mixtures containing a small fraction of anionic lipids in which the zwitterionic lipids help the proper organization of the peptide, whereas the ensuing destabilization with the formation of a fusogenic structure requires more anionic phospholipids. Thus, this destabilization can be further increased by the higher concentration of anionic lipids that exist in the inner cell membrane leaflet. The fusion assay shows that leakage probably corresponds to a perturbation of the membrane and is mainly unspecific, and the fusion activity is much more specific. Furthermore, it is not the fact that a ternary mixture is present that induces those activities, but the presence of a negatively charged lipid, because in zwitterionic ones, even with two or three components, the peptide has a much lower and generally uncorrelated fusion activity. However, there are several data that indicate a stronger interaction in the mixtures containing the anionic and zwitterionic lipids as compared with anionic lipid alone that may be related to the formation of nanoclusters of peptide and anionic lipid where the fusogenic structure formation takes place, indicating that the virus is adapted to the complex lipid composition of the target cell membrane.

Wimley and co-workers have made a remarkable study of this system, both in this peptide[49] and also in other peptides derived from the S glycoprotein.[50,51] Regarding the data obtained for this peptide, there is a fair agreement in most of the conclusions; namely, evidence for $\beta$-sheet aggregation, which is reported in their work from CD data and in the IR study we present here. However, distinct evidence was noted in some points. That is, we have found that the $K_p$ values for membrane systems in the absence of negatively charged phospholipids are extremely low. In addition, a peculiar pattern was obtained for the fluorescence intensity because a decrease in Trp fluorescence intensity was observed, pointing out to a structural alteration or aggregation of the peptide. In the present work, we also show that the SARS-CoV $SARS_{FP}$ peptide is capable of affecting the palisade structure of the membrane through studies of the fluorescence intensity decay of DPH. Although the peptide is not deeply buried in the membrane, as commented above, it is able to affect the lipid milieu from its surface, where it locates down to the hydrophobic core where DPH resides, in this last case leaving the probe exposed to an aqueous-like environment. The peptide perturbs more strongly the bilayer in the case of negatively charged phospholipids, as shown by the fluorescence intensity decay of DPH, both in the gel and in the fluid phospholipid phase. The infrared spectra of the amide I′ region of the fully hydrated peptide did not change with temperature, indicating a high stability of its conformation, where extended $\beta$-strands with strong intermolecular interactions predominated. Moreover, we did not find significant changes on the proportion of the different secondary elements when the peptide was incorporated into membranes of different compositions. This is in agreement with (i) the fluorescence lifetime of the peptide for which only minor changes were observed and (ii) the CD experiments of Sainz et al.[49] that had to reduce significantly the concentration of peptide and measure the spectra in limiting conditions to observe alterations (namely, induction of $\beta$-type structures) upon membrane incorporation, because for typical CD concentrations, the peptide in buffer has already shown propensity for $\beta$-aggregate formation. In addition, it strongly points to a biologically active form of the peptide to be the membrane-bound aggregate because for a very diluted peptide, the membrane induces a structure that is similar to the one in water with higher concentration.[49] In addition, the fluorescence lifetime parameters underwent a less noticeable change for the EPC/BPS/Chol lipid system, which is the one with a stronger interaction with the peptide. This data would suggest that apart from a negatively charged phospholipid, the presence of a more sizable headgroup would be important in the peptide−membrane interaction, perhaps allowing a hydrophobic interaction in a shallow position by protecting the more hydrophobic residues of $SARS_{FP}$ from water. It is interesting to note that the fluorescent form of the peptide in buffer is largely monomeric, as concluded from the fluorescence anisotropy of its Trp residue, whereas in the presence of a membrane, the peptide should be arranged in a somehow regular aggregate. In this case, different Trp residues should be close to each other, protected from interaction with the Lys residues, with a stronger steady-state fluorescence intensity than in water, leading possibly to the formation of a highly fusogenic structure. From the small changes in fluorescence lifetime parameters, it is very reasonable to suppose that although the structure of the peptide is not very different in water and in the membrane-bound form, the way it organizes should be completely different (note that in the membranes in which the fluorescence intensity of the peptide decreases in relation to water, the fusogenic activity is also quite low). It is known that in the case of class I membrane fusion proteins, several fusion peptide fragments pertaining to different trimers can promote the formation of local nipples in the cell membrane, leading to the formation of local bends, which could induce zones of nonlamellar phases on the outer leaflet.[52] It would be possible that to compensate for the imbalance produced by a different phospholipid assembly, phospholipid flip−flop from the inner leaflet to the outer leaflet could be endorsed.[53] The present data would suggest that disassembly of the core could possible happen only after exposure to negatively charged membranes, either by flip−flop or when in contact with the inner leaflet; that is, by making small holes in the outer leaflet, as shown by the short component induced in the fluorescence decay of DPH, which shows up in both negative and neutral lipid membranes. It is quite interesting to notice that the model system used here that most resembles a mammalian plasma membrane outer leaflet (EPC/SM/Chol) is the one inducing a smaller spectral shift, a more noticeable decrease in fluorescence intensity of the peptide, less vesicle aggregation, and no detectable fusion. In this way, the transverse asymmetry of the target cell membrane, which is challenged by the perturbation induced by the peptide in the outer leaflet, becomes of importance for the process. In this way, the region where the SARS-CoV $SARS_{FP}$ peptide is located could interact with the negatively charged leaflet, favoring the fusion process and leading to the fusogenic pore formation.

**Acknowledgment.** This work was supported by Grant BFU2005-00186-BMC (Ministerio de Ciencia y Tecnología, Spain) to J.V. and PTDC/QUI/68151/2006 (Fundação para a Ciência e a Tecnologia, Portugal). J.G. is a recipient of a predoctoral fellowship from the Autonomous Government of the Valencian Community, Spain. R.F.M. de A. was a recipient of a postdoctoral fellowship from F.C.T., Portugal (SFRH/BPD/32210/2006). We are especially grateful to Ana I. Gómez Sanchez and Alexander Fedorov for their excellent technical assistance.

## Appendix

### Abbreviations

| | |
|---|---|
| ANTS | 8-aminonaphthalene-1,3,6-trisulfonic acid |
| 16NS | 16-doxyl-stearic acid |
| 5NS | 5-doxyl-stearic acid |
| BPI | bovine liver L-α-phosphatidylinositol |
| BPS | bovine brain L-α-phosphatidylserine |
| CD | circular dichroism |
| CF | 5-carboxyfluorescein |
| Chol | cholesterol |
| CoV | coronavirus |
| di-8-ANEPPS | 4-(2-(6-(dioctylamino)-2-naphthalenyl)ethenyl)-1-(3-sulfopropyl)-pyridinium inner salt |
| DMPA | 1,2-dimyristoyl-*sn*-glycerophosphatidic acid; |
| DMPC | 1,2-dimyristoyl-*sn*-glycerophosphatidylcholine |
| DMPG | 1,2-dimyristoyl-*sn*-glycerophosphatidylglycerol |
| DMPS | 1,2-dimyristoyl-*sn*-glycerophosphatidylserine |
| DPH | 1,6-diphenyl-1,3,5-hexatriene |
| DPX | *p*-xylene-bis-pyridinium bromide |
| EPA | egg L-α-phosphatidic acid |
| EPC | egg L-α-phosphatidylcholine |
| EPE | egg trans-sterified L-α-phosphatidylethanolamine |
| EPG | egg L-α-phosphatidylglycerol |
| ESM | egg sphingomyelin |
| FP | fusion peptide |

| | |
|---|---|
| FTIR | Fourier-transform infrared spectroscopy |
| HIV-1 | human immunodeficiency virus type 1 |
| HR | heptad repeat region |
| LUV | large unilamellar vesicles |
| MLV | multilamellar vesicles |
| NBD-PE | *N*-(7-nitrobenz-2-oxa-1,3-diazol-4-yl)-1,2-dihexadecanoyl-*sn*-glycero-3-phosphoethanolamine |
| PTM | pretransmembrane domain |
| RhB-PE | *N*-lissamine rhodamine B-1,2-dihexadecanoyl-*sn*-glycero-3- phosphoethanolamine |
| SARS | severe acute respiratory syndrome |
| $SARS_{FP}$ | putative fusion peptide of SARS |
| $T_m$ | main transition temperature |
| TM | transmembrane domain |

## References and Notes


(1) Marra, M. A.; Jones, S. J.; Astell, C. R.; Holt, R. A.; Brooks-Wilson, A.; Butterfield, Y. S.; Khattra, J.; Asano, J. K.; Barber, S. A.; Chan, S. Y.; Cloutier, A.; Coughlin, S. M.; Freeman, D.; Girn, N.; Griffith, O. L.; Leach, S. R.; Mayo, M.; McDonald, H.; Montgomery, S. B.; Pandoh, P. K.; Petrescu, A. S.; Robertson, A. G.; Schein, J. E.; Siddiqui, A.; Smailus, D. E.; Stott, J. M.; Yang, G. S.; Plummer, F.; Andonov, A.; Artsob, H.; Bastien, N.; Bernard, K.; Booth, T. F.; Bowness, D.; Czub, M.; Drebot, M.; Fernando, L.; Flick, R.; Garbutt, M.; Gray, M.; Grolla, A.; Jones, S.; Feldmann, H.; Meyers, A.; Kabani, A.; Li, Y.; Normand, S.; Stroher, U.; Tipples, G. A.; Tyler, S.; Vogrig, R.; Ward, D.; Watson, B.; Brunham, R. C.; Krajden, M.; Petric, M.; Skowronski, D. M.; Upton, C.; Roper, R. L. *Science* **2003**, *300*, 1399.

(2) Rota, P. A.; Oberste, M. S.; Monroe, S. S.; Nix, W. A.; Campagnoli, R.; Icenogle, J. P.; Penaranda, S.; Bankamp, B.; Maher, K.; Chen, M. H.; Tong, S.; Tamin, A.; Lowe, L.; Frace, M.; DeRisi, J. L.; Chen, Q.; Wang, D.; Erdman, D. D.; Peret, T. C.; Burns, C.; Ksiazek, T. G.; Rollin, P. E.; Sanchez, A.; Liffick, S.; Holloway, B.; Limor, J.; McCaustland, K.; Olsen-Rasmussen, M.; Fouchier, R.; Gunther, S.; Osterhaus, A. D.; Drosten, C.; Pallansch, M. A.; Anderson, L. J.; Bellini, W. J. *Science* **2003**, *300*, 1394.

(3) Kan, B.; Wang, M.; Jing, H.; Xu, H.; Jiang, X.; Yan, M.; Liang, W.; Zheng, H.; Wan, K.; Liu, Q.; Cui, B.; Xu, Y.; Zhang, E.; Wang, H.; Ye, J.; Li, G.; Li, M.; Cui, Z.; Qi, X.; Chen, K.; Du, L.; Gao, K.; Zhao, Y. T.; Zou, X. Z.; Feng, Y. J.; Gao, Y. F.; Hai, R.; Yu, D.; Guan, Y.; Xu, J. *J. Virol.* **2005**, *79*, 11892.

(4) Li, W.; Moore, M. J.; Vasilieva, N.; Sui, J.; Wong, S. K.; Berne, M. A.; Somasundaran, M.; Sullivan, J. L.; Luzuriaga, K.; Greenough, T. C.; Choe, H.; Farzan, M. *Nature* **2003**, *426*, 450.

(5) Jeffers, S. A.; Tusell, S. M.; Gillim-Ross, L.; Hemmila, E. M.; Achenbach, J. E.; Babcock, G. J.; Thomas, W. D., Jr.; Thackray, L. B.; Young, M. D.; Mason, R. J.; Ambrosino, D. M.; Wentworth, D. E.; Demartini, J. C.; Holmes, K. V. *Proc. Natl. Acad. Sci. U.S.A.* **2004**, *101*, 15748.

(6) Masters, P. S. *Adv. Virus Res.* **2006**, *66*, 193.

(7) Xiao, X.; Chakraborti, S.; Dimitrov, A. S.; Gramatikoff, K.; Dimitrov, D. S. *Biochem. Biophys. Res. Commun.* **2003**, *312*, 1159.

(8) Howard, M. W.; Tripet, B.; Jobling, M. G.; Holmes, R. K.; Holmes, K. V.; Hodges, R. S. *Adv. Exp. Med. Biol.* **2006**, *581*, 319.

(9) Xu, Y.; Zhu, J.; Liu, Y.; Lou, Z.; Yuan, F.; Liu, Y.; Cole, D. K.; Ni, L.; Su, N.; Qin, L.; Li, X.; Bai, Z.; Bell, J. I.; Pang, H.; Tien, P.; Gao, G. F.; Rao, Z. *Biochemistry* **2004**, *43*, 14064.

(10) Ingallinella, P.; Bianchi, E.; Finotto, M.; Cantoni, G.; Eckert, D. M.; Supekar, V. M.; Bruckmann, C.; Carfi, A.; Pessi, A. *Proc. Natl. Acad. Sci. U.S.A.* **2004**, *101*, 8709.

(11) Gallaher, W. R. *Cell* **1996**, *85*, 477.

(12) Chambers, P.; Pringle, C. R.; Easton, A. J. *J. Gen. Virol.* **1990**, *71* (12), 3075.

(13) Bosch, B. J.; van der Zee, R.; de Haan, C. A.; Rottier, P. J. *J. Virol.* **2003**, *77*, 8801.

(14) Liu, S.; Xiao, G.; Chen, Y.; He, Y.; Niu, J.; Escalante, C. R.; Xiong, H.; Farmar, J.; Debnath, A. K.; Tien, P.; Jiang, S. *Lancet* **2004**, *363*, 938.

(15) Tripet, B.; Howard, M. W.; Jobling, M.; Holmes, R. K.; Holmes, K. V.; Hodges, R. S. *J. Biol. Chem.* **2004**, *279*, 20836.

(16) Zhu, J.; Xiao, G.; Xu, Y.; Yuan, F.; Zheng, C.; Liu, Y.; Yan, H.; Cole, D. K.; Bell, J. I.; Rao, Z.; Tien, P.; Gao, G. F. *Biochem. Biophys. Res. Commun.* **2004**, *319*, 283.

(17) Supekar, V. M.; Bruckmann, C.; Ingallinella, P.; Bianchi, E.; Pessi, A.; Carfi, A. *Proc. Natl. Acad. Sci. U.S.A.* **2004**, *101*, 17958.

(18) Xu, Y.; Lou, Z.; Liu, Y.; Pang, H.; Tien, P.; Gao, G. F.; Rao, Z. *J. Biol. Chem.* **2004**, *279*, 49414.

(19) Epand, R. M. *Biochim. Biophys. Acta* **2003**, *1614*, 116.

(20) Colotto, A.; Epand, R. M. *Biochemistry* **1997**, *36*, 7644.

(21) Siegel, D. P.; Epand, R. M. *Biophys. J.* **1997**, *73*, 3089.

(22) Aranda, F. J.; Teruel, J. A.; Ortiz, A. *Biochim. Biophys. Acta* **2003**, *1618*, 51.

(23) Contreras, L. M.; Aranda, F. J.; Gavilanes, F.; Gonzalez-Ros, J. M.; Villalain, J. *Biochemistry* **2001**, *40*, 3196.

(24) Bernabeu, A.; Guillen, J.; Perez-Berna, A. J.; Moreno, M. R.; Villalain, J. *Biochim. Biophys. Acta* **2007**, *1768*, 1659.

(25) Moreno, M. R.; Guillen, J.; Perez-Berna, A. J.; Amoros, D.; Gomez, A. I.; Bernabeu, A.; Villalain, J. *Biochemistry* **2007**, *46*, 10572.

(26) Perez-Berna, A. J.; Guillen, J.; Moreno, M. R.; Bernabeu, A.; Pabst, G.; Laggner, P.; Villalain, J. *J. Biol. Chem.* **2008**, *283*, 8089.

(27) Böttcher, C. S. F.; Van Gent, C. M.; Fries, C. *Anal. Chim. Acta* **1961**, *1061*, 203.

(28) Edelhoch, H. *Biochemistry* **1967**, *6*, 1948.

(29) de Almeida, R. F.; Borst, J.;. Fedorov, A.;. Prieto, M.; Visser, A. J. *Biophys. J.* **2007**, *93*, 539.

(30) de Almeida, R. F.; Loura, L. M.; Fedorov, A.; Prieto, M. *J. Mol. Biol.* **2005**, *346*, 1109.

(31) De Almeida, R. F.; Loura, L. M.; Prieto, M.; Watts, A.; Fedorov, A.; Barrantes, F. J. *Mol. Membr. Biol.* **2006**, *23*, 305.

(32) Contreras, L. M.; de Almeida, R. F.; Villalain, J.; Fedorov, A.; Prieto, M. *Biophys. J.* **2001**, *80*, 2273.

(33) Giudici, M.; Pascual, R.; de la Canal, L.; Pfuller, K.; Pfuller, U.; Villalain, J. *Biophys. J.* **2003**, *85*, 971.

(34) Pascual, R.; Contreras, M.; Fedorov, A.; Prieto, M.; Villalain, J. *Biochemistry* **2005**, *44*, 14275.

(35) Peisajovich, S. G.; Shai, Y. *Biochim. Biophys. Acta* **2003**, *1614*, 122.

(36) Guillen, J.; Perez-Berna, A. J.; Moreno, M. R.; Villalain, J. *J. Virol.* **2005**, *79*, 1743.

(37) Blumenthal, R.; Clague, M. J.; Durell, S. R.; Epand, R. M. *Chem. Rev.* **2003**, *103*, 53.

(38) Struck, D. K.; Hoekstra, D.; Pagano, R. E. *Biochemistry* **1981**, *20*, 4093.

(39) Meers, P.; Ali, S.; Erukulla, R.; Janoff, A. S. *Biochim. Biophys. Acta* **2000**, *1467*, 227.

(40) Perez-Berna, A. J.; Moreno, M. R.; Guillen, J.; Bernabeu, A.; Villalain, J. *Biochemistry* **2006**, *45*, 3755.

(41) Cladera, J.; Martin, I.; O'Shea, P. *EMBO J.* **2001**, *20*, 19.

(42) O'Shea, P. *Biochem. Soc. Trans.* **2003**, *31*, 990.

(43) Cladera, J.; O'Shea, P. *Biophys. J.* **1998**, *74*, 2434.

(44) Kuntz, I. D., Jr.; Kauzmann, W. *Adv. Protein Chem.* **1974**, *28*, 239.

(45) Zimmerberg, J.; Chernomordik, L. V. *Adv. Drug. Delivery Rev.* **1999**, *38*, 197.

(46) Chernomordik, L. V.; Kozlov, M. M. *Cell* **2005**, *123*, 375.

(47) Guillen, J.; Moreno, M. R.; Perez-Berna, A. J.; Bernabeu, A.; Villalain, J. *J. Phys. Chem. B* **2007**, *111*, 13714.

(48) de Almeida, R. F.; Loura, L. M.; Prieto, M.; Watts, A.; Fedorov, A.; Barrantes, F. J. *Biophys. J.* **2004**, *86*, 2261.

(49) Sainz, B., Jr.; Rausch, J. M.; Gallaher, W. R.; Garry, R. F.; Wimley, W. C. *J. Virol.* **2005**, *79*, 7195.

(50) Sainz, B., Jr.; Mossel, E. C.; Gallaher, W. R.; Wimley, W. C.; Peters, C. J.; Wilson, R. B.; Garry, R. F. *Virus. Res.* **2006**, *120*, 146.

(51) Sainz, B., Jr.; Rausch, J. M.; Gallaher, W. R.; Garry, R. F.; Wimley, W. C. *Biochemistry* **2005**, *44*, 947.

(52) Dimitrov, A. S.; Xiao, X.; Dimitrov, D. S.; Blumenthal, R. *J. Biol. Chem.* **2001**, *276*, 30335.

(53) Janmey, P. A.; Kinnunen, P. K. *Trends Cell Biol.* **2006**, *16*, 538.


JP7118229